Original Article

MOLECULAR METABOLISM

Tubular mitochondrial pyruvate carrier disruption elicits redox adaptations that protect from acute kidney injury

Adam J. Rauckhorst[1,2,3,13], Gabriela Vasquez Martinez[4,13], Gabriel Mayoral Andrade[4], Hsiang Wen[5], Ji Young Kim[6], Aaron Simoni[4], Claudia Robles-Planells[4], Kranti A. Mapuskar[7,8], Prerna Rastogi[9], Emily J. Steinbach[5,7,8], Michael L. McCormick[7,8], Bryan G. Allen[7,8], Navjot S. Pabla[6], Ashley R. Jackson[4,11], Mitchell C. Coleman[7,8,10], Douglas R. Spitz[7,8], Eric B. Taylor[1,2,3,8,12,*], Diana Zepeda-Orozco[4,5,11,]**

ABSTRACT

Objective: Energy-intensive kidney reabsorption processes essential for normal whole-body function are maintained by tubular epithelial cell metabolism. Although tubular metabolism changes markedly following acute kidney injury (AKI), it remains unclear which metabolic alterations are beneficial or detrimental. By analyzing large-scale, publicly available datasets, we observed that AKI consistently leads to downregulation of the mitochondrial pyruvate carrier (MPC). This investigation aimed to understand the contribution of the tubular MPC to kidney function, metabolism, and acute injury severity.

Methods: We generated tubular epithelial cell-specific *Mpc1* knockout (MPC TubKO) mice and employed renal function tests, in vivo renal ^{13}C-glucose tracing, mechanistic enzyme activity assays, and tests of injury and survival in an established rhabdomyolysis model of AKI.

Results: MPC TubKO mice retained normal kidney function, displayed unchanged markers of kidney injury, but exhibited coordinately increased enzyme activities of the pentose phosphate pathway and the glutathione and thioredoxin oxidant defense systems. Following rhabdomyolysis-induced AKI, compared to WT control mice, MPC TubKO mice showed increased glycolysis, decreased kidney injury and oxidative stress markers, and strikingly increased survival.

Conclusions: Our findings suggest that decreased renal tubular mitochondrial pyruvate uptake hormetically upregulates oxidant defense systems before AKI and is a beneficial adaptive response after rhabdomyolysis-induced AKI. This raises the possibility of therapeutically modulating the MPC to attenuate AKI severity.

Keywords Acute kidney injury; Hormesis; Metabolomics; Mitochondrial metabolism; Oxidative stress

1. INTRODUCTION

Acute kidney injury (AKI) is a major societal health problem [1,2]. In hospitalized patients, AKI is associated with increased length of stay, cost, and risk of mortality. Furthermore, survivors of AKI are at risk for greater injury from subsequent renal insults and for developing chronic kidney disease [3,4]. Tubular cell injury is an initiating event in the pathophysiological cascade of AKI. Although mechanisms of tubular injury are diverse, altered mitochondrial function and increased oxidative stress are common features. Tubular cells are rich in mitochondria that support ATP production to maintain their energy-intensive reabsorption processes. The high metabolic rate and

[1]Department of Molecular Physiology and Biophysics, University of Iowa, Iowa City, IA, USA [2]Fraternal Order of Eagles Diabetes Research Center (FOEDRC), University of Iowa, Iowa City, IA, USA [3]FOEDRC Metabolomics Core Research Facility, University of Iowa, Iowa City, IA, USA [4]Kidney and Urinary Tract Research Center, The Abigail Wexner Research Institute at Nationwide Children's Hospital, Columbus OH, USA [5]Stead Family Department of Pediatrics, University of Iowa, Iowa City, IA, USA [6]Division of Pharmaceutics and Pharmacology, College of Pharmacy & Comprehensive Cancer Center, The Ohio State University, Columbus, OH, USA [7]Free Radical and Radiation Biology Program, Department of Radiation Oncology, University of Iowa, Iowa City, IA, USA [8]Holden Comprehensive Cancer Center, University of Iowa, Iowa City, IA, USA [9]Department of Pathology, University of Iowa, Iowa City, IA, USA [10]Department of Orthopedics and Rehabilitation, University of Iowa, Iowa City, IA, USA [11]Department of Pediatrics, The Ohio State University, Columbus, OH, USA [12]Pappajohn Biomedical Institute, University of Iowa, Iowa City, IA, USA

[13] Adam J. Rauckhorst and Gabriela Vasquez Martinez contributed equally to this work.

*Corresponding author. Department of Molecular Physiology and Biophysics, 169 Newton Rd. 3316 Pappajohn Biomedical Discovery Building, University of Iowa, Iowa City, IA, 52242, USA. E-mail: eric-taylor@uiowa.edu (E.B. Taylor).

**Corresponding author. Kidney and Urinary Tract Research Center, The Abigail Wexner Research Institute at Nationwide Children's Hospital, 700 Children's Drive, W325, Columbus, OH, 43205, USA; E-mail: diana.zepeda-orozco@nationwidechildrens.org (D. Zepeda-Orozco).

Received April 19, 2023 • Revision received November 28, 2023 • Accepted November 30, 2023 • Available online 7 December 2023

https://doi.org/10.1016/j.molmet.2023.101849

mitochondrial content of tubular cells in-turn confers a high vulnerability to secondary oxidative injury following a primary insult (reviewed in [5–7]). Thus, understanding the relationship between tubular cell mitochondrial energetics and redox processes is critical to develop improved methods of attenuating AKI.

Mitochondrial pyruvate oxidation is a central feature of kidney metabolism, regulates redox balance, and is decreased during AKI [8–12]. All tubular segments utilize pyruvate for mitochondrial metabolism derived primarily from circulating lactate and secondarily from glycolysis [13,14]. Conversion of lactate to pyruvate in route to mitochondrial oxidation generates cytosolic NADH, and oxidation of glycolytically produced pyruvate decreases glucose availability for NADPH production by the pentose phosphate pathway (PPP). Within mitochondria, pyruvate oxidation provides NADH and FADH2 that energize the electron transport chain (ETC) and drive oxidative phosphorylation for bulk ATP production. However, when mitochondria are dysfunctional, pyruvate oxidation can contribute to dysregulated ETC activity as a primary producer of cytotoxic reactive oxygen species (ROS). Under conditions of pathological ROS, channeling glucose into the PPP is cytoprotective by generating the NADPH required as cofactor for the glutathione and thioredoxin antioxidant systems. Thus, during AKI glucose, lactate, and pyruvate metabolism must be coordinated to minimize ROS-dependent cellular damage while maintaining adequate energy production. However, the mechanisms leading to the decreased mitochondrial pyruvate oxidation during and how they contribute to AKI are not well understood.

The mitochondrial pyruvate carrier (MPC) regulates the fate of glucose and lactate by transporting their common product pyruvate into mitochondria for TCA cycle oxidation. The MPC is a mitochondrial inner-membrane protein complex formed by two obligate subunits, MPC1 and MPC2 [15,16]. Studies of MPC disruption in diverse systems illustrate a conserved metabolic adaptive program where glucose and lactate oxidation decrease, glycolysis increases, and TCA cycle glutamine oxidation increases [17–24]. In some cases, this contributes to disease, such as in many cancers where MPC disruption augments the Warburg effect [25,26]. Conversely, in others, MPC disruption is beneficial, such as in adult skeletal muscle and liver, where it attenuates type 2 diabetes [27–30]. Notably, in the liver, which like the kidney has profound capacity to oxidize glutamine, the increased glutamine oxidation caused by MPC disruption competes with glutathione synthesis and adaptively increases glutathione turnover through the transsulfuration pathway [31]. Thus, the MPC occupies a nexus of metabolism, impacting energetics, substrate preference, and ROS defense systems, and can be therapeutically disrupted in some tissues [27–30]. However, the role of the MPC in normal kidney metabolism and in response to AKI, which is distinctively marked by decreased pyruvate oxidation and increased oxidative stress, is poorly defined.

Here, we address the role of the MPC in basic kidney tubule metabolism and AKI. Data from publicly available, large-scale datasets corroborated by our own experiments showed that the MPC is downregulated after AKI, raising the question of how decreased MPC activity affects AKI severity. To investigate this, we generated novel kidney tubule epithelial cell-specific MPC knockout (MPC TubKO) mice and implemented a rhabdomyolysis model of AKI. Under normal conditions, MPC TubKO decreased glucose, lactate, and pyruvate influx into TCA cycle metabolites and increased glucose influx into the PPP, NADPH levels, and glutathione turnover and reduction state. MPC TubKO strikingly increased survival from rhabdomyolysis-induced AKI, which was accompanied by decreased ROS-mediated tubular injury. Our findings demonstrate a central role of the kidney tubular cell MPC in metabolic regulation. They suggest that MPC TubKO protects from rhabdomyolysis-induced AKI by both hormetically upregulating PPP activity and enhancing the metabolic switch to glycolysis during injury. These data provide an example of how modulating mitochondrial carbon fuel transport can protect from AKI, highlighting the potential therapeutic value of targeting mitochondrial transporters to protect from metabolic injury.

2. MATERIALS AND METHODS

2.1. Mice breeding

All animal care and procedures were conducted in adherence to the National Institute of Health Guide for the Care and Use of Laboratory Animals. Studies were approved by the Nationwide Children's Hospital (protocol #AR20-00055) and the University of Iowa (protocol #8041235-004) Institutional Animal Care and Use Committees. *Mpc1*$^{f/f}$ mice, generated as previously described [27], were crossed to tubule specific Pax8-Cre (Jackson Laboratory, 028196) [32,33] generating [*Pax8*$^{Cre+/-}$*Mpc1*$^{f/f}$ (MPC TubKO)] and controls [*Pax8*$^{Cre-/-}$*Mpc1*$^{f/f}$ (WT)]. ROSA$^{mT/mG}$ (Jackson Laboratory, 007676) were crossed with mice expressing Cre under the control of the gamma-glutamyltransferase promoter (Ggt1-Cre) as previously described [34]. All mice were maintained on a C57Bl6J background and *Mpc1*$^{f/f}$ mice were backcrossed to WT C57Bl6J at least 10 generations prior to use.

2.2. Animal models of AKI

Ischemia reperfusion (IR)-, cisplatin-, and rhabdomyolysis-induced AKI were applied to male mice aged 8–12 weeks using methods previously described [35–38]. Briefly, to cause ischemia-reperfusion injury, kidneys of isoflurane anesthetized mice were exposed and bilateral renal pedicles were clamped for 30 min. Following clamp removal, sutures closed the muscle and skin around the incision. The sham groups underwent a similar procedure but without bilateral clamping. Cisplatin-induced nephrotoxicity was trigged by a single intraperitoneal cisplatin (30 mg/kg) injection as described previously [37], and the sham (vehicle) group was injected with equal volumes of normal saline. To induce rhabdomyolysis, mice were intramuscularly injected with 50% glycerol (Sigma, G7893, dose 7.5–10 mL/kg) to the two hind-legs, and the sham group was injected with equal volumes of normal saline. For all injury models, kidneys were dissected from ad libitum fed, anesthetized mice and snap frozen within 2–3 min for non-metabolomic analytical work.

2.3. Renal function

Blood samples were collected via submandibular bleed into BD Microtainer tubes with serum separator additive (BD 365967), stored on ice for at 15 min, and centrifuged at 1200 rpm for 2 min at room temperature to obtain serum, which was stored at −80 °C until use. Serum Cystatin C levels were measured using the Mouse/Rat Cystatin C Quantikine enzyme-linked immunosorbent assay (ELISA) kit (R&D Systems, MSCTC0). Blood Nitrogen Urea serum levels were measured using the QuantiChrom Urea Assay Kit (BioAssay Systems, DIUR-100).

2.4. Uniformly labeled ([U−^{13}C])-glucose and [U−^{13}C]-lactate/-pyruvate in vivo tracing

7 - 8- or 10 - 12-week-old WT and MPC TubKO mice were fasted for 4 h prior to intraperitoneal injection with uniformly labeled [U−^{13}C]-glucose (10% ^{13}C-glucose, 2.0 g/kg lean body mass, Cambridge Isotope) or uniformly labeled [U−^{13}C]-lactate/-pyruvate (10:1, 3.0 g/kg lean body mass, Cambridge Isotope), respectively. For tracing during

acute kidney injury, rhabdomyolysis-induced injury was induced as described above and after 6 h mice were injected with [U—^{13}C]-glucose. 30 min after injection mice were anesthetized using a pre-determined time course of isoflurane administration. The abdomen of the anesthetized mice was opened exposing the kidneys. A single kidney was isolated, dissected, and frozen within 30 s using a liquid N_2 cooled freeze-clamp [39]. Freeze-clamped tissues were processed for LC-MS as described in the Supplemental Methods. Kidneys harvested from mice treated with natural abundance lactate/pyruvate were used to correct for ^{13}C natural abundance [40]. Metabolite identification is described in the Supplemental Methods.

2.5. Activity assays

For all enzymatic activity assays, whole kidney tissue including cortex and medulla was homogenized in DETAPAC buffer comprising 0.05 M phosphate buffer, pH 7.8, 1.34 mM DETAPAC, and protein levels were determined using the Lowry assay. The assays were performed on a Beckman DU 800 spectrophotometer.

2.5.1. MnSOD activity assay

SOD activity was determined using the indirect competitive inhibition assay as described previously [41]. Briefly, the flux of superoxide generated by the reaction of xanthine & xanthine oxidase was measured using nitroblue tetrazolium (NBT). Increasing concentrations of SOD rapidly converts the superoxide produced to hydrogen peroxide and the rate of NBT reduction is inhibited and can be measured spectrophotometrically at 560 nm. The rate of NBT reduction is calculated as percent inhibition, relative to the NBT reduction in the absence of the sample and the amount of protein causing 50% maximum inhibition is defined as one unit of activity. MnSOD activity was distinguished from CuZSOD activity using 5 mmol/L NaCN as described [41].

2.5.2. Glutathione reductase (GR) activity

GR activity was determined by the method of Ray and Prescott [42]. Briefly, sample was diluted into a reaction mixture containing 70 mM KPi, pH 7.6, with 2.4 mM EDTA, 0.1% BSA, 94 μM NADPH, and 1 mM GSSG. The loss of NADPH was assessed at room temperature by monitoring the change in absorbance at 340 nm.

2.5.3. Thioredoxine reductase (TRR) activity

TRR activity was determined using a commercially available kit (Sigma, CS0170) performed according to the supplied instructions.

2.5.4. Glucose 6 phosphate dehydrogenase (G6PD)

G6PD activity was measured using the method of Glock and McLean [43]. Briefly, kidney homogenate was added to a solution containing 75 mM Tris, pH 8.0, with 0.75 mM $MgCl_2$, 1.5 mM $NADP^+$, and 1.2 mM glucose 6-phosphate. G6PD activity was determined by the rate of NADPH formation at 340 nm. To ensure the specificity of G6PD activity measurement, homogenates were also run in the presence of 1.2 mM 6-phosphogluconic acid, with and without glucose 6-phosphate.

2.5.5. Citrate synthase activity

Citrate synthase activity was measured using the protocol previously described [44]. A sample volume equivalent to 50 μg of protein was combined with 0.5 mM oxaloacetic acid, and 0.1 mM dTNB. The formation of TNB was monitored at 412 nm every 30 min for 2 h. Regression analysis was used to determine reaction rates.

2.5.6. Mitochondrial ETC activities

Measurements of the ETC complex activities were done as described previously [45]. Complex I activity was assayed as the rate of rotenone-inhibitable NADH oxidation at 340 nm with 425 nm as reference. Samples were assayed with or without 200 μg/mL rotenone in working buffer containing 25 mM potassium phosphate buffer, 5 mM magnesium chloride, 2 mM potassium cyanide, 2.5 mg/mL BSA, 0.13 mM NADH, 200 μg/mL antimycin A, 7.5 mM coenzyme Q1. Complex II activity was assayed as the rate of reduction of 2,6-dichloroindophenol by coenzyme Q in the presence and absence of 0.2 M succinate at 600 nm. Samples were incubated with or without succinate in 25 mM potassium phosphate buffer, 5 mM magnesium chloride, 2 mM potassium cyanide, 2.5 mg/mL BSA for 10 min at 30 C. After incubation, 200 μg/mL antimycin A, 200 μg/mL rotenone, 5 mM DCIP, and 7.5 mM coenzyme Q1 were added to each cuvette and incubated for 1 min before reading absorbance rates. Complex III activity was assayed as the rate of cytochrome c reduction by coenzyme Q2 at 550 nm with 580 nm as reference. Samples were assayed in 25 mM potassium phosphate buffer, 5 mM magnesium chloride, 2 mM potassium cyanide, 2.5 mg/mL BSA, 0.5 mM n-dodecyl β-maltoside, 200 μg/mL rotenone, 1.5 mM cytochrome c, and 3.5 mM coenzyme Q2.

2.6. Statistics

Data are presented as the mean ± SEM. Statistical analysis was performed using GraphPad Prism 8 and 9 (GraphPad Software). An unpaired t test was used to compare differences between 2 groups. Multiple-group comparisons were performed using one- or two-way ANOVA with the Holm-Sidak multiple comparison test. Differences were considered statistically significant when a P value was less than 0.05.

2.7. Additional methods

Additional methods can be found in the Supplemental Document.

3. DATA AVAILABILITY

3.1. Lead contact

Additional information and requests for reagents and resources should be directed to and will be fulfilled by the lead contacts, Dr. Diana Zepeda-Orozco (diana.zepeda-orozco@nationwidechildrens.org) and Dr. Eric Taylor (eric-taylor@uiowa.edu).

3.2. Materials availability

No new materials were generated during this study.

4. RESULTS

4.1. Mpc1 is expressed in proximal and distal tubular segments and is decreased in AKI

Mitochondrial pyruvate oxidation impacts cellular redox state through multiple pathways and is decreased in AKI [8—11]. Because mitochondrial pyruvate uptake gates pyruvate oxidation, changes in tubular MPC activity could contribute to the decreased pyruvate oxidation and redox perturbations from AKI. To examine this, we first queried publicly available RNAseq datasets and observed tubular *Mpc1* mRNA abundance to be significantly downregulated following cisplatin-, ischemia reperfusion-, and rhabdomyolysis-induced AKI (Supplemental Figure 1A, B) [46,47]. To test the reproducibility of these results, we implemented similar mouse models of each. We found that, in addition to *Mpc1* mRNA, MPC1 protein levels were significantly decreased 48 h after cisplatin-, ischemia-reperfusion-,

rhabdomyolysis-induced AKI (Figure 1A–C, Supplemental Figure 1C). Because rhabdomyolysis-induced AKI decreased MPC1 protein the most among the models tested, we extended our analysis of rhabdomyolysis-injured tissue. Immunofluorescence analysis showed that tubular MPC1 protein was primarily decreased in the cortico-medullary junction with a prominent decrease in the distal tubular segments (Figure 1D). Widespread cell death was not observed, consistent with the decrease in MPC protein content being a regulated cellular event. We then generated mT/mG/Ggt1-Cre reporter mice that express membrane-localized GFP in renal tubular epithelial cells (RTECs), whereas all other cell-types express membrane-localized tdTomato (Figure 1E). RTECs showed significantly decreased *Mpc1* mRNA and MPC1 protein abundance following rhabdomyolysis-induced AKI, which remained unchanged in Non-RTECs (Figure 1F,G). VDAC protein levels were unaffected by injury, demonstrating that the decreased RTEC MPC1 abundance occurred independent of changes in total mitochondrial content (Figure 1G).

4.2. Generation and characterization of MPC TubKO mice

To test the role of the MPC in the kidney tubule in vivo, we generated *Mpc1* pan-tubular epithelial cell knock out mice (MPC TubKO) by crossing *Mpc1*$^{f/f}$ mice with *Pax8-Cre* mice (Figure 2A). MPC TubKO mice were viable at birth, and at 8 weeks of age they displayed normal body weight and levels of the renal function marker Cystatin C (Figure 2B, C). *Mpc1* mRNA was decreased by greater than 90% in MPC TubKO kidney tissue, which propagated to similar decreases in both MPC1 and MPC2 protein content (Figure 2D–G). We performed immunofluorescence staining across tubular segments to identify potential regions with residual MPC1 protein (Figure 2H). Compared to WT controls, MPC1 in MPC TubKO mice was nearly absent in the proximal tubule cells of the renal cortex and corticomedullary junction and decreased but not eliminated in the corresponding distal tubules. Pax8 is reported to be expressed in the developing brain and liver [32,48]. To test for *Mpc1* deletion in brain and liver, we measured mRNA and protein abundance in these tissues from WT and MPC TubKO mice. Compared to WT controls, *Mpc1* mRNA and MPC1 protein

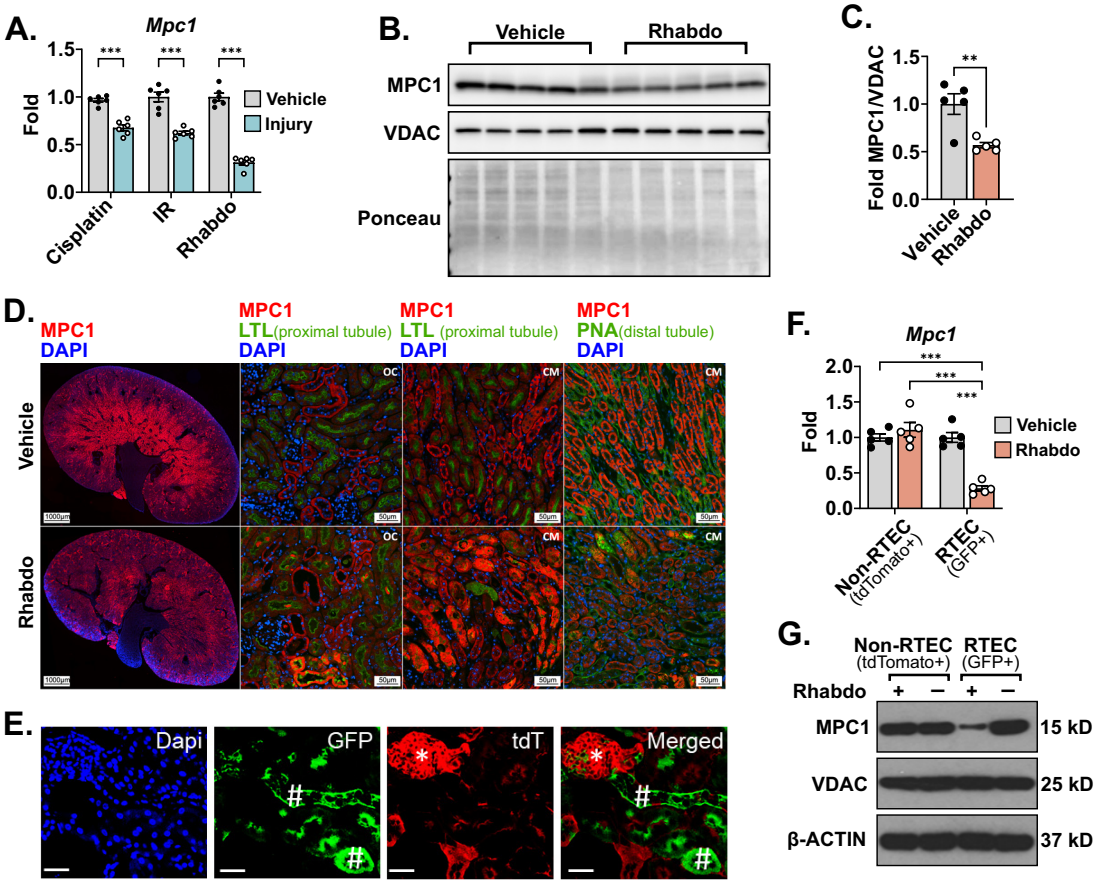

Figure 1: Mpc1 is expressed in proximal and distal tubular segments and is decreased in AKI. (**A**) Bar graph comparing kidney *Mpc1* mRNA levels after vehicle treatment or cisplatin-, ischemia reperfusion (IR)-, or rhabdomyolysis (Rhabdo)-induced AKIs. Samples were collected 72 h after cisplatin injury and 24 h after IR and rhabdomyolysis injuries. ($n = 6$/group; ***$p < 0.001$ by unpaired t test). (**B**) Representative Western blot of kidney MPC1 protein abundance 24 h after rhabdomyolysis-induced AKI. VDAC was blotted as a loading control and ponceau staining of the membrane is shown. ($n = 5$, **$p < 0.01$ by unpaired t test). (**C**) Quantification of VDAC normalized MPC1 protein abundance after rhabdomyolysis-induced AKI. ($n = 5$, **$p < 0.01$ by unpaired t test). (**D**) Representative immunostaining images of MPC1 (red), lotus tetragonolobus lectin (LTL, green, proximal tubule marker), or peanut agglutinin (PNA, green, distal tubule marker), and DAPI (blue) in whole kidney, outer cortex (OC) and cortico-medullary junction (CM) kidney sections 30 h following vehicle treatment or rhabdomyolysis-induced AKI. (Images captured at 15× magnification; whole kidney scale bar = 1,000 μm; OC and CM scale bar = 50 μm). (**E**) Representative fluorescence image of kidney sections of mT/mG/Ggt1-Cre mice confirming GFP + renal tubular epithelial cells (green, #, GFP) and tdTomato + non-RTEC cells (red, *, tdT) stained with Dapi (blue). (Scale bar = 100 μm). (**F**) Bar graph comparing *Mpc1* mRNA levels in flow-sorted Non-RTEC (tdTomato+) and RTEC (GFP+) cells 24 h after vehicle treatment or rhadbomyolysis-induced AKI. ($n = 5$/group, ***$p < 0.001$ by unpaired t test). (**G**) Representative Western blot of MPC1 and VDAC protein abundance in flow-sorted Non-RTEC (tdTomato+) and RTEC (GFP+) cells 24 h after rhabdomyolysis-induced AKI. β-ACTIN was blotted as a loading control. Data are presented as means ± SEM.

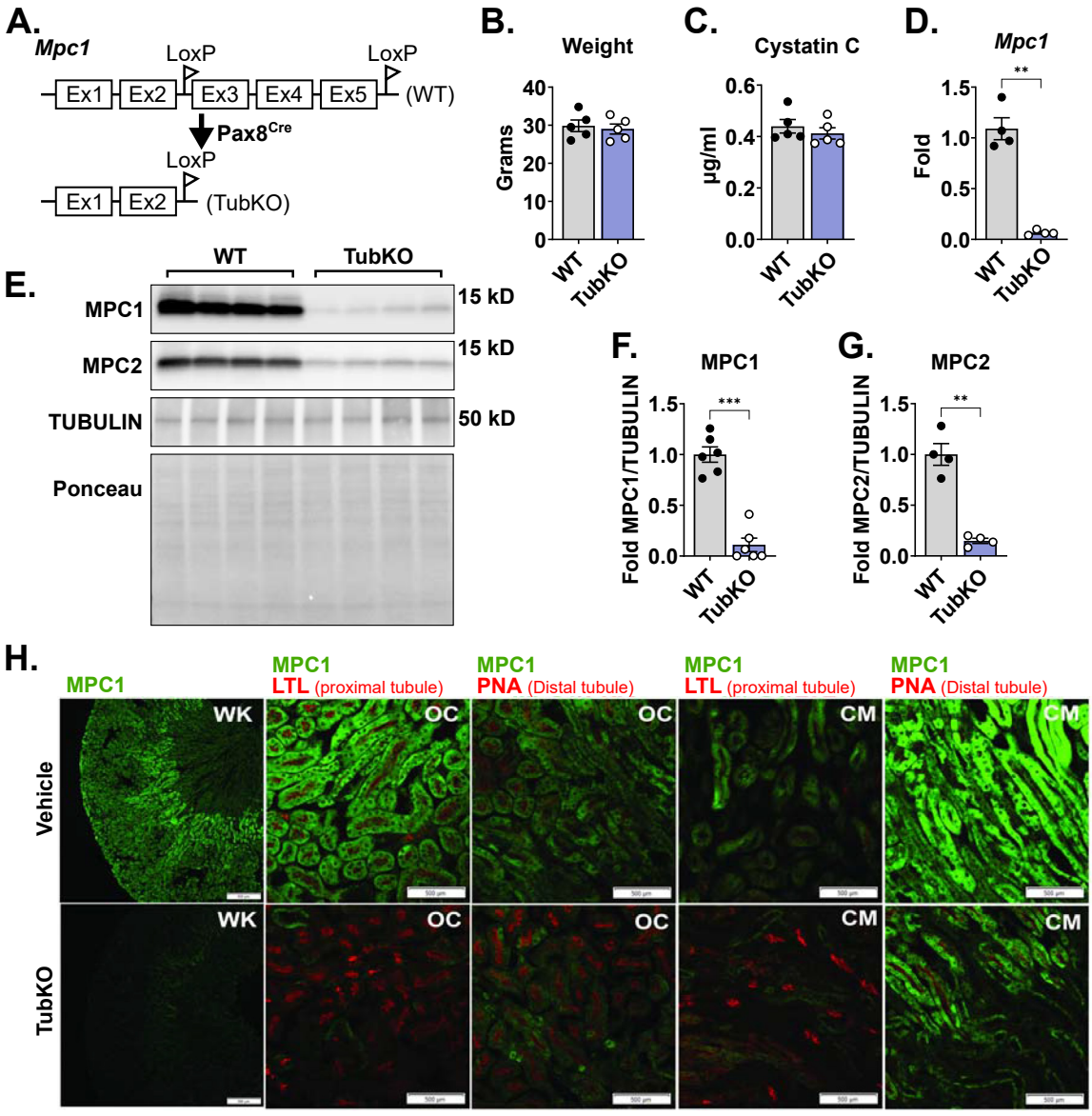

Figure 2: Generation and characterization of MPC TubKO mice. (A) Schematic illustrating the generation of tubular *Mpc1* null allele mice (MPC TubKO). **(B–C)** Bar graphs showing body weights (**B**) and serum cystatin C concentration (**C**) in WT and MPC TubKO mice. (n = 5/group, 8-week-old mice). **(D)** Bar graph comparing mouse kidney *Mpc1* mRNA levels in WT and MPC TubKO mice. (n = 4/group, 7 - 12-week-old mice, $^{**}p < 0.01$ by unpaired t test). **(E–G)** Representative Western blot of kidney MPC1 and MPC2 protein abundance (**E**) and quantification of normalized MPC1 (**F**) and MPC2 (**G**) protein levels in WT and MPC TubKO mice. Tubulin was blotted as loading control and used as the protein quantification normalizer. Ponceau staining of the membrane is shown. (n = 4–6/group, 7 - 12-week-old mice, $^{**}p < 0.01$ and $^{***}p < 0.001$ by unpaired t test). **(H)** Representative immunostaining images of kidney MPC1 (green) and lotus tetragonolobus lectin (LTL, green, proximal tubule marker) or peanut agglutinin (PNA, green, distal tubule marker) in the whole kidney (WK), outer-cortex (OC), and cortico-medullary junction (CM) in WT and MPC TubKO mice. (Images taken at 4× (WK) or 20× (OC and CM) magnification, scale bar = 500 µm). Data are presented as means ± SEM.

levels were similar in the brains and livers of MPC TubKO, consistent with tubular cell-delimited MPC knockout (Supplemental Figure 2A-F).

4.3. Tubular Mpc1 deletion decreases cellular pyruvate oxidation and perturbs ETC function

Next, we considered how tubular cell MPC loss affects bioenergetics. We surveyed the mitochondrial oxygen consumption effects of MPC inhibition by UK5099, a well-described MPC inhibitor [49], in the LLC-PK1 pig kidney tubular epithelial cell line. When pyruvate was supplied as the sole oxidative fuel, MPC inhibition significantly decreased oligomycin-dependent proton leak and FCCP-dependent maximal respiration (Figure 3A). In previous reports on non-kidney systems, MPC loss adaptively increases glutamine metabolism to maintain mitochondrial metabolite levels and drive electron transport chain (ETC) conductance [18,20]. Here, when glutamine was supplied as the substrate, LLC-PK1 cell O_2 consumption rates did not change with MPC inhibition (Figure 3B). This was in contrast to isolated kidney mitochondria, where MPC TubKO increased glutamine oxidation rates, which may signify adaptation to chronic MPC loss (Supplemental Figure 3A). Fatty acid oxidation is a quantitatively important fuel for kidney energy production [50] and in prior reports increased with MPC disruption in C2C12 myoblasts, liver, and skeletal muscle

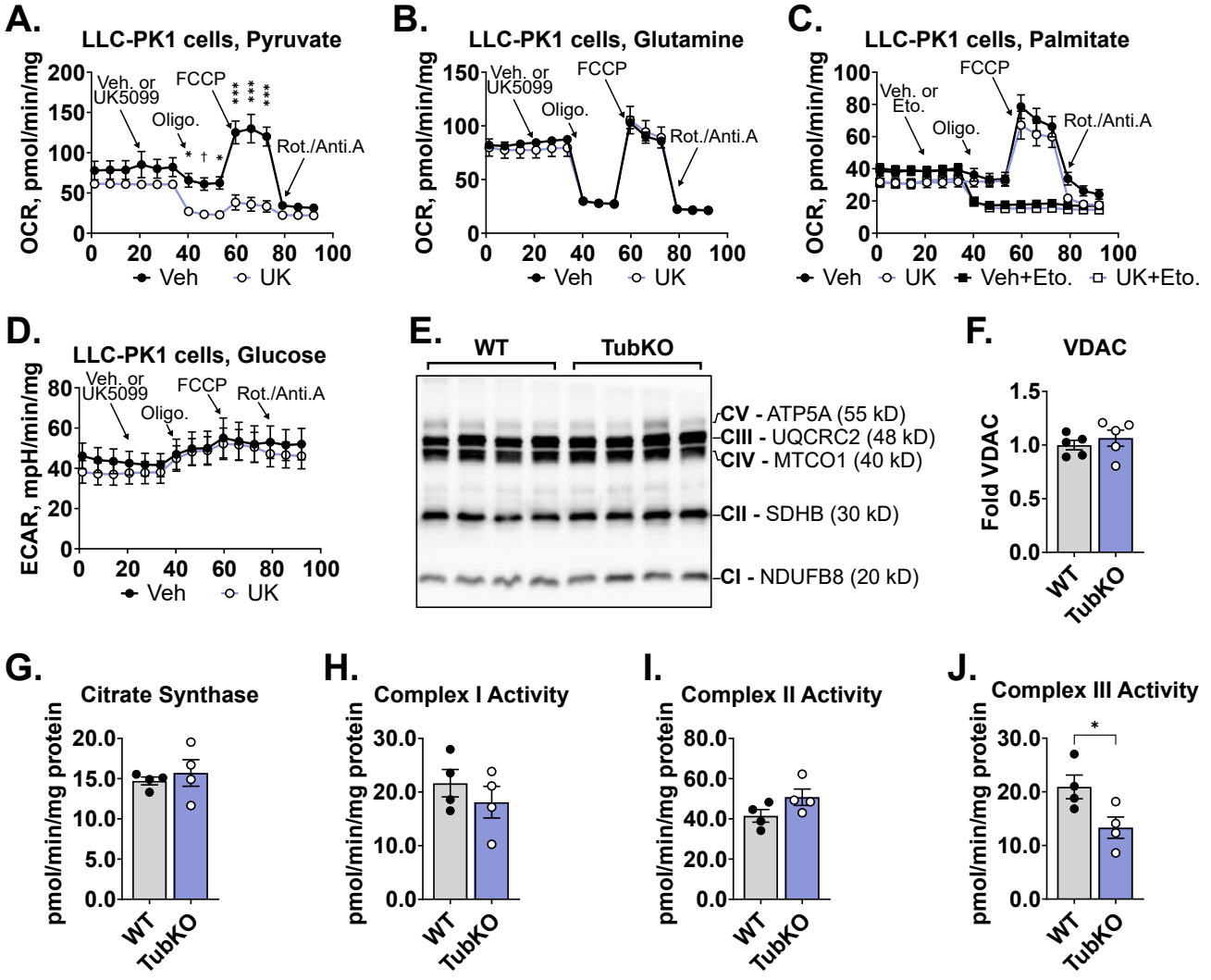

Figure 3: Tubular Mpc1 deletion decreases cellular pyruvate oxidation and perturbs ETC function. (**A-C**) Line graph showing the oxygen consumption rate of LLC-PK1 cells provided with (**A**) pyruvate, (**B**) glutamine, or (**C**) palmitate + glucose as substrates. Inhibitors were added as indicated. Veh., Vehicle; Oligo., Oligomycin; Rot./Anti.A, Rotenone/Antimycin A;, Eto., Etomoxir. ($n = 5-12$, †$p < 0.1$, *$p < 0.05$, ***$p < 0.001$ by two-way ANOVA with the Holm-Sidak multiple comparison test within measurement). (**D**) Line graph showing the extracellular acidification rate of LLC-PK1 cells provided with glucose and pyruvate. Inhibitors added as indicated. ($n = 12$). (**E**) Representative Western blot of kidney ETC marker Complex I (CI), NDUFB8; Complex II (CII), SDHB; Complex III (CIII), UQCRC2; Complex IV (CIV), MTCO1; and Complex V (CV), ATP5A protein abundances in WT and MPC TubKO mice. ($n = 4$/group, 6 - 8-week-old mice). (**F**) Bar graph comparing the quantified VDAC protein level in WT and MPC TubKO mice. ($n = 5$/group, 6 - 8-week-old mice). (**G-J**) Bar graphs comparing the whole-kidney enzymatic activities of citrate synthase (**G**), Complex I (**H**), Complex II (**I**), and Complex III (**J**) in WT and MPC TubKO mice. ($n = 4$/group, 6-week-old mice, *$p < 0.05$ by unpaired t test). Data are presented as means ± SEM.

[17,27,28,30]. Here, UK5099-treated LLC-PK1 cells oxidized palmitate at similar rates to vehicle treated cells (Figure 3C). We then examined the extracellular acidification rates of vehicle- or UK5099-treated LLC-PK1 cells as a measure of glycolytic activity. We found these to be unchanged, suggesting that acute MPC inhibition does not alter glycolytic rates and that LLC-PK1 cells may maintain essential energetics with basal levels of glycolysis and mitochondrial oxidation of glutamine and fatty acids (Figure 3D). Next, we assessed VDAC protein levels and citrate synthase activity in whole kidney extracts as markers of mitochondrial content and found no differences between MPC TubKO mice and WT controls (Figure 3E–G, Supplemental Figure 3B). Similarly, no apparent differences were detected in markers of ETC protein abundance (Figure 3E). Given that each ETC complex comprises multiple subunits and that individual ETC protein levels do not denote enzymatic activities, we biochemically evaluated ETC Complex I, II, and III activities. Complex I and complex II activities were similar between MPC TubKO and WT controls (Figure 3H, I). However, MPC TubKO complex III activity was significantly decreased, suggesting that MPC loss may downregulate the ETC, which could alter ROS production (Figure 3J) [51]. Together, these data suggest tubular MPC disruption directly affects mitochondrial function without altering cellular mitochondrial content.

4.4. Tubular MPC disruption leads to upregulation of oxidant defense systems

To identify metabolic changes evoked by tubular MPC disruption, we compared the steady-state metabolomic profiles of freeze-clamped WT and MPC TubKO kidney tissue. The relative abundances of 49 metabolites were significantly different (Figure S4A, Supplemental Table 1). While pyruvate was not significantly increased, lactate and

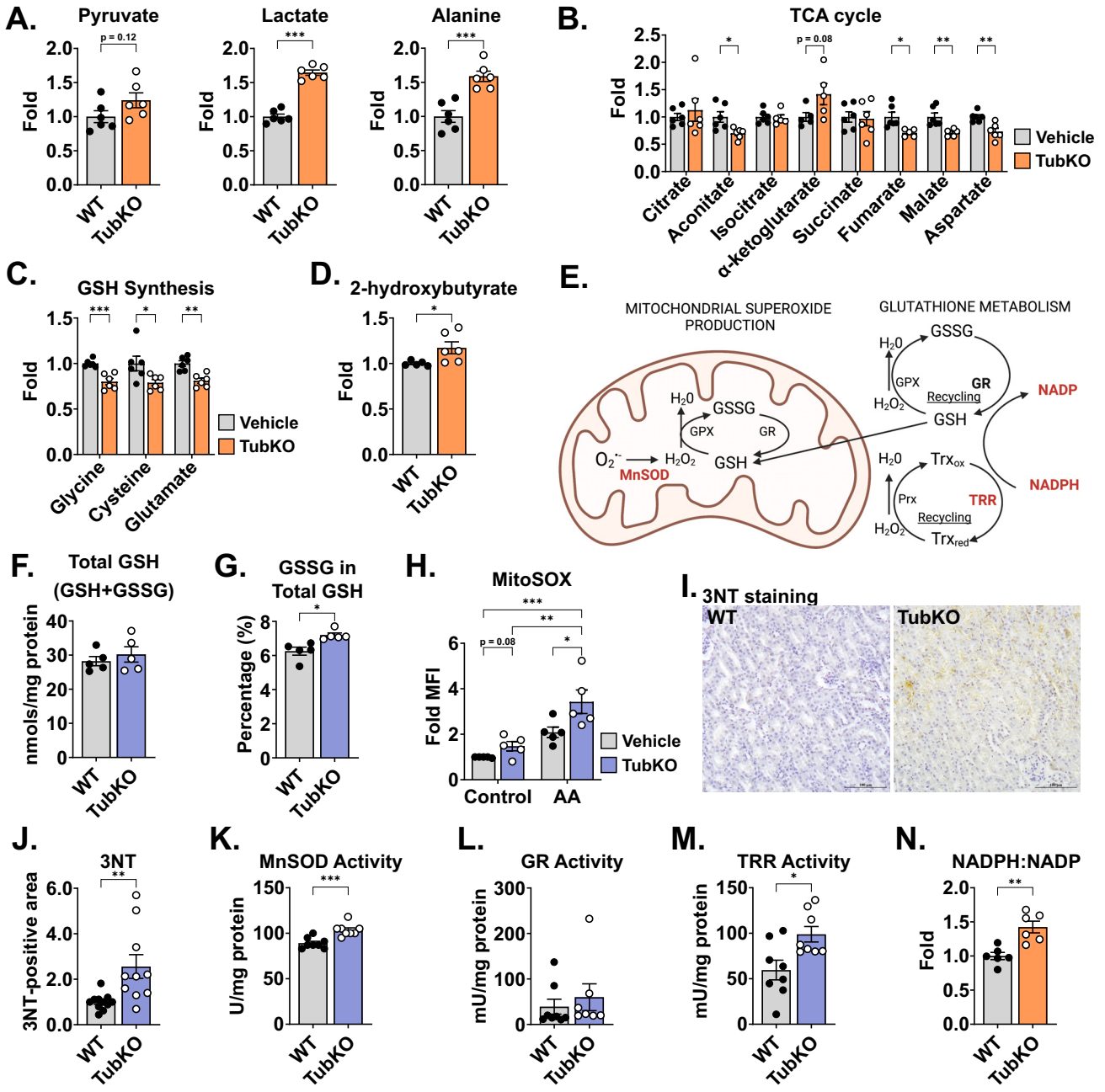

Figure 4: Tubular MPC disruption leads to upregulation of oxidant defense systems. (**A-D**) Bar graphs showing kidney metabolite levels in WT and MPC TubKO mice. Pyruvate, lactate, and alanine (**A**), TCA cycle metabolites (**B**), GSH synthesis substrates glycine, cysteine, and glutamate (**C**), and 2-hydroxybutyrate, a marker of GSH turnover (**D**). (n = 6/group, 8 - 12-week-old mice, *p < 0.05, **p < 0.01, and ***p < 0.001 by unpaired t test). (**E**) Schematic illustrating mitochondrial antioxidant defense system including MnSOD, manganese superoxide dismutase; GSH, glutathione; GSSG, oxidized glutathione; GPX, glutathione peroxidase; GR, glutathione reductase; Prx, peroxiredoxin; TRR, thioredoxin reductase; Trx_{red}, reduced thioredoxin; and Trx_{ox}, and oxidized thioredoxin. (**F-G**). Bar graphs comparing kidney total GSH (GSH + GSSG) (**F**) and the % of GSSG of total GSH (GSH + GSSG) (**G**) in WT and MPC TubKO mice. (n = 5/group, 12 - 14-week-old mice, *p < 0.05 by unpaired t test). (**H**) Bar graph showing MitoSOX oxidation in the presence and absence of antimycin A (AA) of isolated WT and MPC TubKO tubular epithelial cell. The y-axis shows the fold mean fluorescence intensity (MFI). (n = 5/group, 12-week-old mice, *p < 0.05, **p < 0.01, ***p < 0.001 by two-way ANOVA with the Holm-Sidak multiple comparison test). (**I**) Representative immunohistochemistry images of kidney 3NT staining in WT and MPC TubKO mice. (Images taken at 40× magnification, scale bar = 100 μm). (**J**) Bar graph comparing kidney 3NT quantification in WT and MPC TubKO mice. (n = 8–11, 12 - 14-week-old mice, **p < 0.01 by unpaired t test). (**K-M**) Bar graphs showing kidney enzyme activities of MnSOD (**K**), GR (**L**), and TRR (**M**) in WT and MPC TubKO mice. (n = 7–8/group, 12 - 14-week-old mice, *p < 0.05 and ***p < 0.001 by unpaired t test). (**N**) Bar graph comparing the kidney NADPH:NADP ratio in WT and MPC TubKO mice. (n = 6/group, 8 - 12-week-old mice, **p < 0.01 by unpaired t test). Data are presented as means ± SEM.

alanine, which are produced from pyruvate by single metabolic reactions and were previously identified to be increased in models of MPC disruption [28,29,39], were significantly increased in MPC TubKO kidneys (Figure 4A). TCA cycle metabolites were broadly decreased except for α-ketoglutarate, which is consistent with decreased pyruvate and increased glutamine oxidation (Figure 4B). Notably, MPC TubKO kidneys had decreased levels of the glutathione (GSH) synthesis substrates glycine, cysteine, and glutamate (Figure 4C) and increased levels of 2-hydroxybutyrate, a marker of glutathione turnover [31,52,53] (Figure 4D). These data indicate that tubular MPC loss elicits metabolic adaptation, including changes to central carbon and glutathione metabolism.

Based on these metabolomic changes, we analyzed the transcript abundance of related enzymes. Transcript levels of glutathione synthase (*Gss*) were significantly decreased with MPC loss, but glutamate-cysteine ligase subunits (*Gclc*) and (*Gclm*) were unchanged (Supplemental Figure 4B). Glycolytic hexokinase1 (*Hk1*), phosphofructose kinase (*Pfkp*), and lactate dehydrogenase (*Ldha*) transcript levels were unchanged (Supplemental Figure 4C). No differences were observed in transcript levels of enzymes involved in fatty acid oxidation like acyl-CoA oxidase 1 (*Acox1*) and hydroxyacyl-CoA dehydrogenase trifunctional enzyme (*Hadha*), glutaminase (*Gls*), or glutamate dehydrogenase (*Glud*) (Supplemental Figure 4D,E). Lastly, we measured transcript abundance for glutamate-pyruvate transaminase 1 (*Gpt1*) and malic enzyme 1 (*Me1*), which catalyze cytosolic pyruvate-alanine and pyruvate-malate interconversions, respectively [27,28,54]. *Me1* levels were significantly decreased in MPC TubKO mice, while *Gpt1* levels were unchanged (Supplemental Figure 4F). These data demonstrate that under basal conditions MPC loss minimally affects transcript levels of key metabolism genes.

Glutathione is the most abundant cellular antioxidant, a key factor in redox signaling, a modulator of cell fate and function (reviewed in [55]), and an integral component for hydroperoxide and electrophile detoxification (Figure 4E). Because our metabolomic profiling data showed changes in glutathione metabolism, we measured total and oxidized glutathione (GSSG) levels using an enzyme-coupled reaction in whole kidney lysates from WT and MPC TubKO mice. Total glutathione levels (GSH + GSSG) were not different (Figure 4F); however, the amount of GSSG in the total glutathione pool (GSH + GSSG) was increased in the MPC TubKO mice, consistent with increased glutathione synthesis and turnover (Figure 4G).

Our finding that MPC TubKO mice have decreased complex III (Figure 3J) activity and an altered glutathione oxidation state (Figure 4G) led us to speculate that loss of the tubular MPC could increase ROS levels and alter cellular redox homeostasis. To test this, we isolated primary tubular cells from MPC TubKO and WT mice and measured mitochondrial ROS production. Superoxide-dependent MitoSOX oxidation in MPC TubKO tubular cells trended towards increased under basal conditions and was significantly increased with complex III inhibitor antimycin A treatment (Figure 4H). Next, we measured the kidney levels of 3-nitrotyrosine (3NT), which is formed from peroxynitrite (ONOO-: the product of $O_2\bullet^-$ + •NO) reacted with tyrosine residues and is a representative marker of oxidative protein modification. MPC TubKO mice had increased 3NT levels (Figure 4I, J). These data indicate that that tubular MPC loss increases reactive oxygen species production.

We expanded our studies to the effects of tubular MPC loss on mitochondrial redox response and cellular oxidant defense systems. As a first step of oxidant defense, aberrant ETC-generated superoxide undergoes dismutation to hydrogen peroxide by manganese superoxide dismutase (MnSOD; SOD2) (Figure 4E). MPC TubKO mice had increased MnSOD activity compared to WT controls (Figure 4K). Next, we looked downstream to the GSH regenerating activity of glutathione reductase (GR), which reduces hydrogen peroxide to water thereby detoxifying ROS. GR activity was mildly, but not significantly increased in MPC TubKO mice (Figure 4L, $p = 0.15$). Thioredoxin (Trx) provides a second thiol redox couple (Trx_{ox}-Trx_{red}) sustained by thioredoxin reductase (TRR) that maintains cellular hydrogen peroxide levels in parallel to GR (Figure 4E). Thioredoxin reductase activity was significantly increased in MPC TubKO mice (Figure 4M). Glutathione reductase and thioredoxin reductase catalysis require NADPH oxidation to NADP (Figure 4E). Consistent with increased support for glutathione reductase and thioredoxin reductase activity, we found increased NADPH and, inversely, decreased NADP with MPC TubKO (Supplemental Figure 4G) resulting in an increased NADPH/NADP ratio in MPC TubKO mice (Figure 4N). This suggests that tubular MPC disruption leads to coordinated increases in NADPH redox cycling and activation of the glutathione and thioredoxin oxidant defense systems.

4.5. MPC TubKO mice have decreased glucose oxidation, exhibit increased PPP activity, and upon injury are better able to switch to glycolytic metabolism

The pentose phosphate pathway (PPP) is the major source of NADPH regeneration in many systems. Thus, we considered whether increased PPP activity could contribute to the increased NADPH/NADP ratio and help sustain the increased activities of the glutathione and thioredoxin antioxidant systems in MPC TubKO mice. To address this, we traced uniformly labeled ([U−^{13}C])-glucose 30 min after a bolus injection into PPP metabolites in WT and TubKO mice, during non-injured control conditions and after rhabdomyolysis-induced AKI (Figure 5A,B). M+6 glucose 6-phosphate, M+6 6-phosphogluconate, and M+5 Ribulose/Ribose 5-phosphate ^{13}C-enrichments were increased in MPC TubKO vs WT under control conditions while pool sizes were unchanged (Figure 5C–E, Supplemental Table 2). In contrast, increased ^{13}C-enrichment after rhabdomyolysis injury in MPC TubKO vs WT was only observed in glucose 6-phosphate (Figure 5C). In WT mice, rhabdomyolysis injury led to increased M+6 glucose 6-phosphate and M+5 Ribulose/Ribose 5-phosphate ^{13}C-enrichments (Figure 5C, E). These data suggest that under non-injured conditions tubular MPC loss increases glucose flux into the PPP that upregulates ROS defenses before injury and eases the metabolic burden for PPP activation after injury.

Because it can operate freely of mitochondrial oxidative phosphorylation and concomitant risk of ROS generation, glycolysis is an important energy source during AKI [8,9,12]. We extended our evaluation of glucose fluxes to glycolysis. We examined ^{13}C-enrichments into fructose 6-phosphate, a metabolite of proximal glycolysis downstream of PPP shunting, and pyruvate and lactate, terminal glycolytic metabolites. In non-injured but not rhabdomyolysis-injured MPC TubKO vs WT mice, M+6 fructose 6-phosphate and M+3 pyruvate ^{13}C-enrichments were significantly increased (Figure 5F–G). Notably, M+3 lactate ^{13}C-enrichment was increased with rhabdomyolysis injury, which was further elevated by MPC loss (Figure 5H). Moreover, lactate abundance was increased in rhabdomyolysis-injured MPC TubKO mice. These data demonstrate that MPC TubKO amplifies the increased glycolysis resulting from rhabdomyolysis AKI.

In contrast to increased glycolysis, MPC disruption is expected to decrease mitochondrial glucose oxidation. Under non-injured conditions, MPC TubKO non-significantly decreased M+2 acetyl-CoA ^{13}C-enrichment and significantly decreased total acetyl-CoA abundance (Figure 5I). This result was matched by decreased M+2,3 citrate, fumarate, malate, and aspartate (oxaloacetate surrogate) ^{13}C-

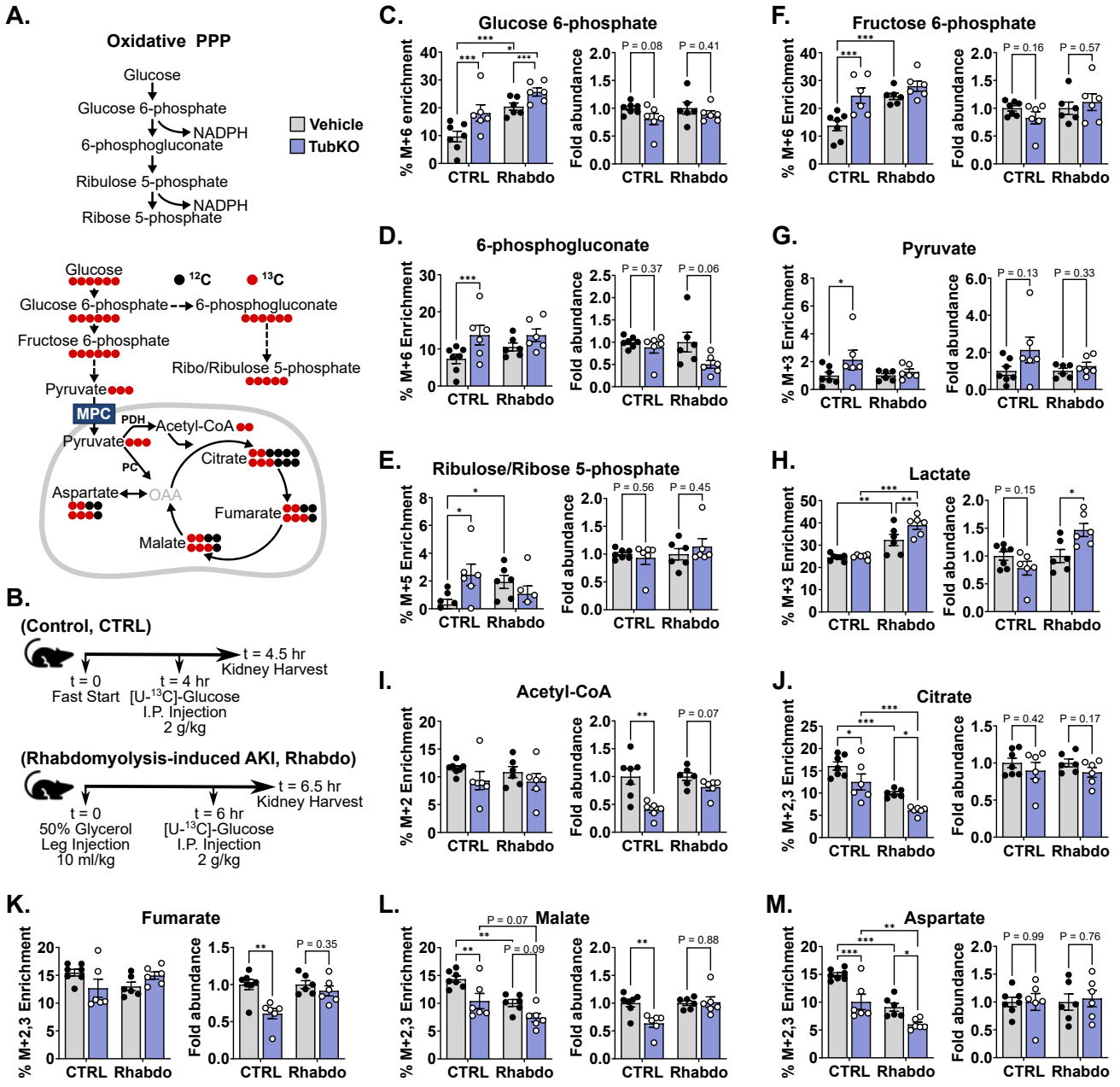

Figure 5: MPC TubKO mice decrease glucose oxidation, increase PPP activity, and upon injury are better able to switch to glycolytic metabolism. (**A**) Schematics illustrating pentose phosphate pathway (PPP) (top) and ^{13}C-enrichment patterns into glycolysis, the PPP, and the TCA cycle from ^{13}C-glucose (bottom). MPC, mitochondrial pyruvate carrier; PDH, pyruvate dehydrogenase; PC, pyruvate carboxylase; OAA, oxaloacetate. (**B**) Schematics illustrating the experimental design for in vivo uniformly labeled [U−^{13}C]-glucose tracing experiments under control and rhabdomyolysis-induced AKI conditions. (**C-M**) Bar graphs showing kidney ^{13}C-isotopologue enrichments and metabolite abundances 30 min after [U−^{13}C]-glucose bolus injection in control (CTRL) and rhabdomyolysis-injured (Rhabdo) WT and MPC TubKO mice. (**C-E**) Pentose phosphate pathway metabolites (**C**) Glucose 6-phosphate, (**D**) 6-phosphogluconate, and (**E**) Ribulose/Ribose 5-phosphate. (**F**−**H**) Glycolytic intermediate metabolites (**F**) Fructose 6-phosphate, (**G**) Pyruvate, and (**H**) Lactate. (**I-M**) TCA cycle intermediate metabolites (**I**) Acetyl-CoA, (**J**) Citrate, (**K**) Fumarate, (**L**) Malate, and (**M**) Aspartate. (n = 7/group, 7 - 8-week-old mice, *p < 0.05 and **p < 0.01, ***p < 0.001 by two-way ANOVA with the Holm-Sidak multiple comparison test (% Enrichment) or by unpaired t test (Fold abundance)). Data are presented as means ± SEM.

enrichments (Figures 5J−M). Consistent with mitochondrial pyruvate uptake being the modulated metabolic control point with MPC disruption, a similar result to the latter was observed when uniformly labeled [U−^{13}C]-lactate/-pyruvate were co-administered and traced (Supplemental Figure 5B-C). Rhabdomyolysis injury decreased M+2,3 ^{13}C-enrichments into citrate, malate, and aspartate in WT mice, which was further increased by MPC TubKO (Figure 5J−M). Residual TCA cycle intermediate ^{13}C-enrichments in MPC TubKO likely resulted from alanine-bypass activity as demonstrated in other MPC loss models [27,28,54]. While the kidney has a role in systemic glucose homeostasis via gluconeogenesis and glucose reabsorption, tubular MPC deletion did not impact systemic blood glucose or lactate levels, following an 18 h fast or in response to a bolus injection of lactate/pyruvate (Supplemental Figure 5D-I). These data demonstrate that MPC TubKO augments the decreased mitochondrial pyruvate oxidation resulting from rhabdomyolysis AKI.

4.6. MPC TubKO mice are protected from ROS mediated damage

Because tubular MPC loss upregulated the glutathione and thioredoxin antioxidant systems and increased PPP glucose influx under basal conditions, we sought to understand how MPC TubKO impacts the PPP enzymatic activity response to AKI. We again utilized rhabdomyolysis-induced AKI, where ROS-dependent injury causes pan-tubular damage (Figure 6A) [56]. First, we examined the activities of the NADPH-producing PPP enzymes glucose 6-phosphate dehydrogenase (G6PD) and 6-phosphogluconate dehydrogenase (6PGDH) (Figure 6B). Twenty-four hours after rhabdomyolysis injury MPC TubKO kidney G6PD activity was significantly increased (Figure 6C) and 6PGDH trended towards increased ($p = 0.07$, Figure 6D). To test if NADPH utilizing oxidant defense systems were upregulated, we examined the activities of glutathione reductase and thioredoxin reductase. Indeed, following injury, MPC TubKO mice more robustly upregulated glutathione reductase and thioredoxin reductase activities (Figure 6E, F). Finally, MPC TubKO mice showed blunted rhabdomyolysis-induced tubular protein glutathionylation, which is a stable marker of cellular oxidative stress [57,58] (Figure 6G, H). These data provide a mechanistic metabolome-to-enzyme activity-basis for how tubular MPC loss protects from oxidative stress during injury.

4.7. MPC TubKO mice are protected from rhabdomyolysis induced kidney injury

Finally, we extended our investigation to test the effect of MPC TubKO in clinical-translational outcomes following rhabdomyolysis-induced AKI. MPC TubKO markedly increased overall survival through 48 h of injury (100% vs 63.6%, $p = 0.05$, $n = 11$ WT and 9 MPC TubKO) (Figure 7A). Furthermore, the renal function markers cystatin C and blood urea nitrogen (BUN), which were similar before injury, were lower in MPC TubKO mice 24 and 48 h after AKI (Figure 7B, C). MPC TubKO mice similarly showed decreased transcript levels of the kidney tubular injury markers *Ngal* and *Kim1* 24 h after AKI (Figure 7D,E), and the histologically assessed tubular injury score 24 h after AKI was decreased (Figure 7F). As a basic measure of cellular stress, we observed decreased tubular apoptosis assessed by tunel staining in MPC TubKO mice 24 h after injury (Figure 7G). These results demonstrate that tubular MPC loss improves multiple markers of kidney injury and protects against rhabdomyolysis-induced tubular injury and AKI mortality.

To statistically summarize how MPC TubKO modulates the glutathione and thioredoxin antioxidants systems during AKI, we correlated all rhabdomyolysis-induced AKI injury data. In WT mice, the degree of

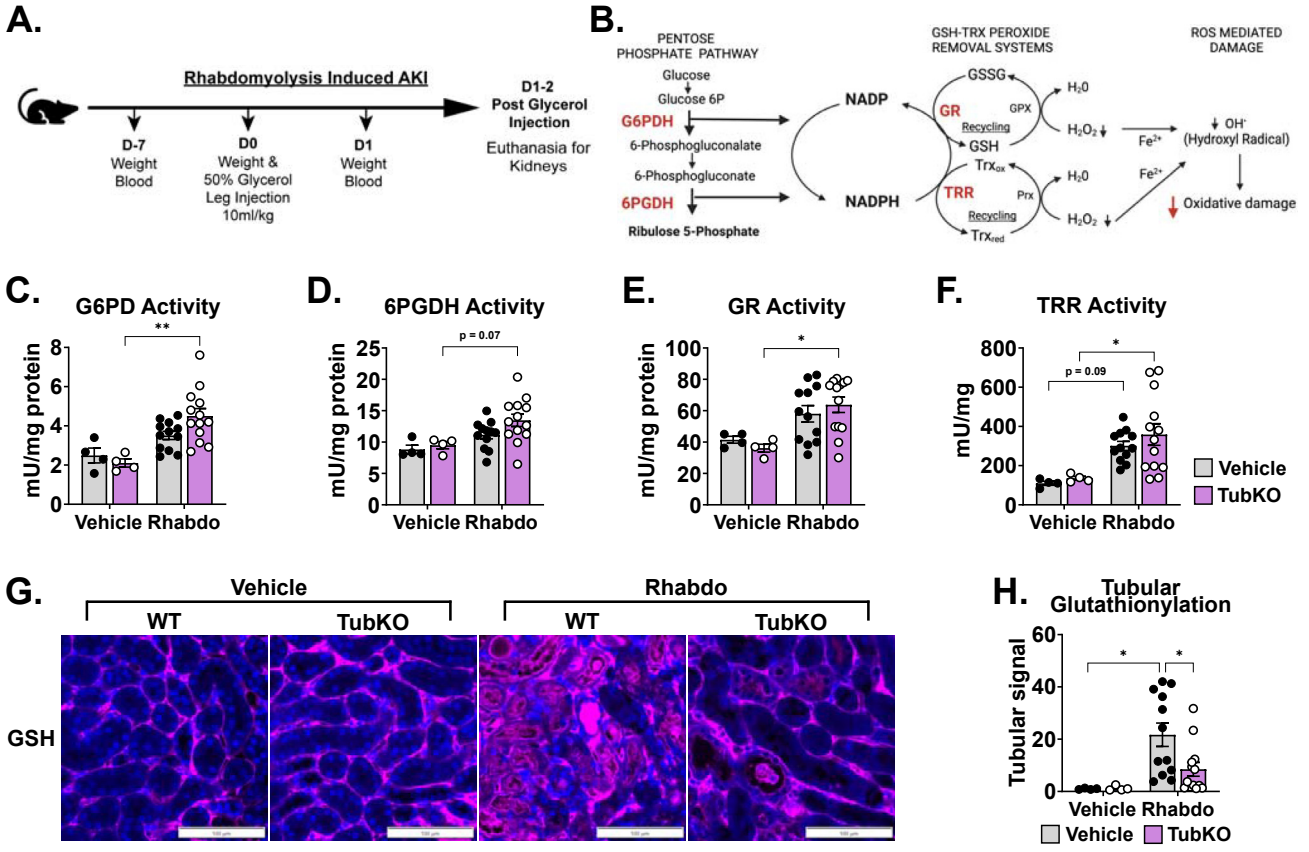

Figure 6: MPC TubKO mice are protected from rhabdomyolysis induced kidney injury. (**A-B**) Schematics illustrating the time course of the rhabdomyolysis-induced AKI model (**A**) and the interconnectedness of the pentose pathway and cellular antioxidant defense systems (**B**). G6PD, glucose 6-phosphate dehydrogenase; 6PGDH, 6-phosphogluconate dehydrogenase; GR, glutathione reductase; TRR, thioredoxin reductase. (**C**–**F**) Bar graphs showing kidney enzyme activities following vehicle treatment or rhabdomyolysis-induced AKI (Rhabdo). G6PD (**C**), 6PGDH (**D**), GR (**E**), and TRR (**F**). ($n = 4$/group for vehicle treatment, $n = 12$–13/group for Rhabdo, 8 - 12-week-old mice, $^*p < 0.05$ and $^{**}p < 0.01$ by two-way ANOVA with the Holm-Sidak multiple comparison test). (**G**) Representative immunostaining images of kidney protein-glutathionylation (pink) and Dapi (blue) following vehicle treatment or rhabdomyolysis-induced AKI in WT and MPC TubKO mice. (Scale bar = 100 μm, $n = 4$/group for vehicle treatment, $n = 12$–13/group for Rhabdo, 8 - 12-week-old mice). (**H**) Bar graph quantifying kidney protein-glutathionylation following vehicle treatment or rhabdomyolysis-induced AKI in WT and MPC TubKO mice. ($n = 4$/group for vehicle treatment, $n = 12$–13/group for Rhabdo, 8–12 week-old mice, $^*p < 0.05$ by two-way ANOVA with the Holm-Sidak multiple comparison test). Data presented as means ± SEM.

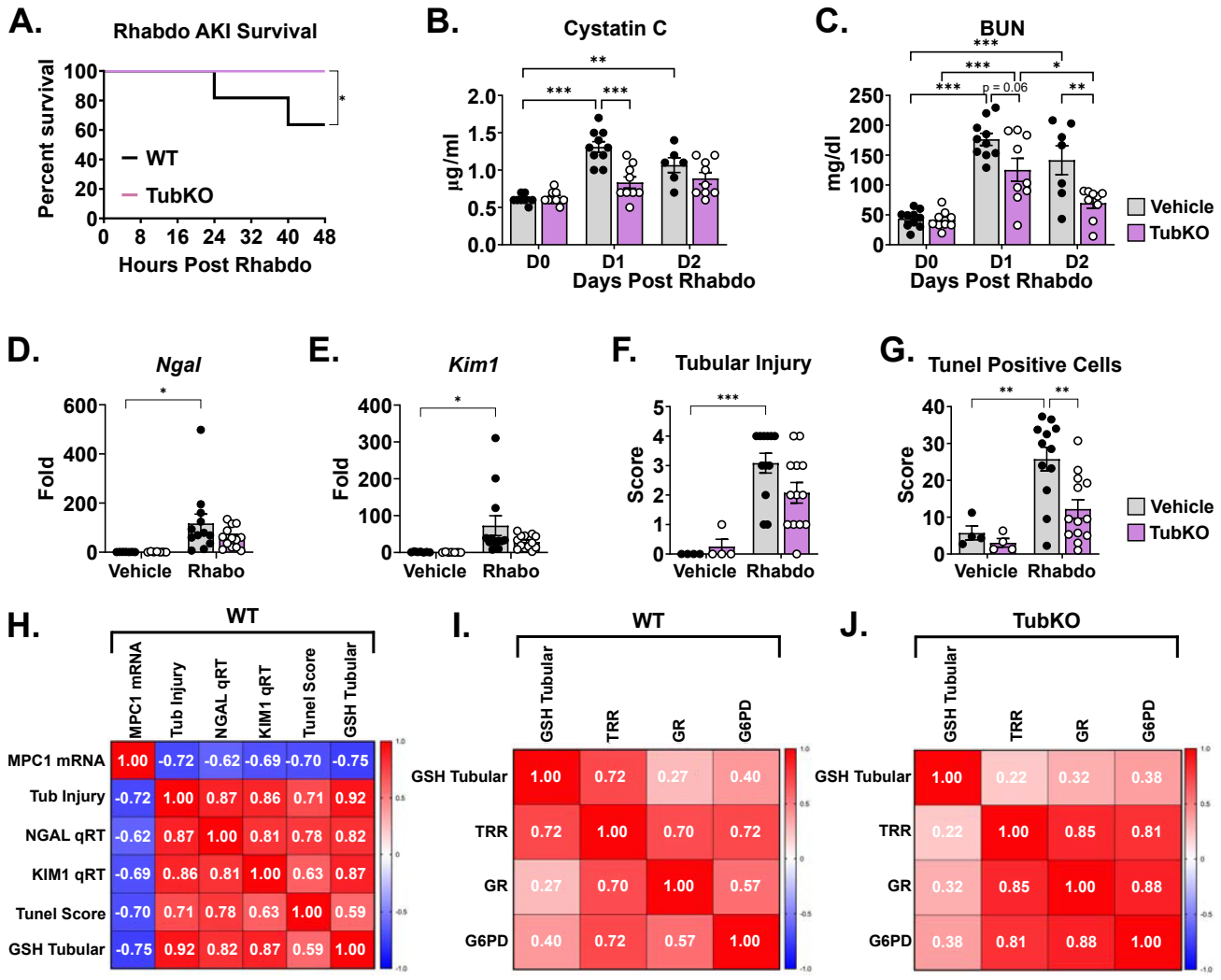

Figure 7: Tubular MPC1 genetic deletion protects from rhabdomyolysis induced kidney injury. (**A**) Line graph showing the survival curve of WT and MPC TubKO mice following rhabdomyolysis-induced AKI (Rhabdo). ($n = 10–11$/group, 8 - 12-week-old mice, $^{*}p < 0.05$ by Mantel–Cox log-rank test). (**B–C**) Bar graphs showing serum cystatin C (**B**), and blood urea nitrogen (**C**, BUN) levels prior to (D0) and on day 1 (D1, 24-hours) and day 2 (D2, 48 h) after vehicle treatment or rhabdomyolysis-induced AKI in WT and MPC TubKO mice. ($n = 10–11$/group, 8–12 week-old mice, $^{*}p < 0.05$, $^{**}p < 0.01$, $^{***}p < 0.001$ by two-way ANOVA followed by the Holm-Sidak multiple comparison tests). (**D-E**) Bar graphs showing kidney *Ngal* (**D**) and *Kim1* (**E**) mRNA levels one day (24 h) after vehicle treatment or rhabdomyolysis-induced AKI in WT and MPC TubKO mice. ($n = 4$/group for vehicle treatment, $n = 12–13$/group for Rhabdo, 8 - 12-week-old mice, $^{*}p < 0.05$ by two-way ANOVA with the Holm-Sidak multiple comparison test). (**F-G**) Bar graphs showing quantification of histologically assessed tubular injury score (**F**) and tunel positive tubular cells (**G**) one day (24 h) after vehicle treatment or rhabdomyolysis-induced AKI in WT and MPC TubKO mice. ($n = 4$/group for vehicle treatment, $n = 12–13$/group for Rhabdo, 8 - 12-week-old mice, $^{**}p < 0.01$ and $^{***}p < 0.001$ by two-way ANOVA with the Holm-Sidak multiple comparison test). (**G-J**) Heatmaps showing Spearman correlation between variables analyzed following vehicle treatment or rhabdomyolysis-induced AKI. Correlation calculated in WT mice comparing *Mpc1* mRNA levels, tubular injury, *Ngal* and *Kim1* mRNA levels, tunel score, and tubular GSH with AKI (**H**). Spearman correlation performed in WT (**I**) and MPC TubKO (**J**) mice comparing GSH and antioxidant defense system markers following rhabdomyolysis-induced AKI. Data are presented as means ± SEM.

Mpc1 mRNA decrease inversely correlated with the degree of tubular GSH ($r = -0.75$, $p = 0.001$), tubular injury ($r = -0.72$, $p = 0.002$), tunel score ($r = -0.70$, $p = 0.004$), and tubular injury biomarkers *Ngal* ($r = -0.62$, $p = 0.0125$) and *Kim1* ($r = -0.69$, $p = 0.004$) mRNA abundance (Figure 7H). Thioredoxin reductase activity positively correlated with tubular GSH in WT mice ($r = 0.72$, $p = 0.002$) which was lost in MPC TubKO mice ($r = 0.22$, $p = 0.4$) (Figure 7I, J). Glucose 6-phosphate dehydrogenase activity and thioredoxin reductase and glutathione reductase more strongly correlated in MPC TubKO mice ($r = 0.81$ and 0.88, $p < 0.001$) compared to WT controls ($r = 0.72$ and 0.57, $p = 0.002$ and 0.024 respectively) showing that MPC TubKO mice have an increased capacity to maintain tubular redox state and increased PPP activity following AKI.

5. DISCUSSION

Kidney metabolic changes following AKI including increased glycolysis and decreased mitochondrial pyruvate oxidation are well described [8–11]. However, the mechanisms regulating mitochondrial pyruvate oxidation after AKI and how pyruvate oxidation capacity affects AKI severity are not well defined. We found that MPC1 mRNA and protein levels are decreased in renal tubular epithelial cells (RTECs) following cisplatin-, ischemia reperfusion-, and rhabdomyolysis-induced AKI. Given this observation, we aimed to test the contribution of the tubular MPC to basic kidney metabolism and rhabdomyolysis-induced AKI severity. Our overall findings demonstrate that the MPC regulates tubular mitochondrial pyruvate oxidation in vivo and that MPC

disruption induces upregulation of antioxidant systems, amplifies the metabolic switch to glycolysis upon injury, and protects from rhabdomyolysis-induced AKI.

This investigation demonstrates that the MPC plays a central role in tubular metabolism that is also dispensable for basic kidney function. Given the enormous energetic demands required for kidney function and the decreased pyruvate oxidation observed after AKI, a key question is how decreased pyruvate oxidation impacts kidney function. Tubular epithelial cells rely on mitochondrial activity to perform a variety of functions including ATP production, solute reabsorption, gluconeogenesis, ammoniagenesis, redox balance, and calcium signaling among others (reviewed in [59]). Our observations that serum cystatin C, BUN, and tubular injury markers *Ngal* and *Kim1* were normal in uninjured MPC TubKO mice suggest that tubular cell metabolic adaptations to MPC loss are sufficient to maintain normal function and do not cause overt kidney injury.

Our results illustrate how tubular MPC disruption changes glucose metabolism before and after rhabdomyolysis injury. Stable isotope tracing in vivo in WT and MPC TubKO mice, before and after rhabdomyolysis AKI, show that MPC disruption decreased glucose flux into the TCA cycle and thus mitochondrial pyruvate oxidation. This result was corroborated ex vivo by respirometry experiments with cultured pig kidney epithelial LLC-PK1 cells showing that acute MPC inhibition with UK5099 decreased pyruvate oxidation. Because the kidney generates the majority of its energy from fatty acid oxidation, which requires mitochondrial oxaloacetate [50], we tested how acute MPC inhibition affected fatty acid oxidation in LLC-PK1 cells. We observed no significant effects of acute MPC inhibition on fatty acid oxidation. This result suggests that essential pyruvate oxidation and anaplerosis enabling fatty acid oxidation persisted after MPC disruption. Partial maintenance of pyruvate oxidation and TCA cycle anaplerosis, in vivo and ex vivo, likely occurs by a combination of pyruvate-alanine cycling that bypasses the MPC and increased glutaminolysis that provides a non-glucose-derived, MPC-independent mitochondrial fuel source [18,27,28,31,54].

MPC TubKO increased glucose flux into the PPP before injury and into lactate production after rhabdomyolysis AKI. In the non-injured state, [U—^{13}C]-glucose tracing showed that MPC TubKO kidneys had increased glucose 6-phosphate, 6-phosphogluconate, and ribulose/ribose 5-phosphate ^{13}C-enrichments. [U—^{13}C]-glucose tracing after rhabdomyolysis AKI showed that MPC TubKO increased M+3 lactate ^{13}C-enrichment and lactate abundance. Notably, lactate ^{13}C-enrichment and abundance were increased in WT mice, but the effect was greater in MPC TubKO mice, indicating an amplified glycolytic response to injury. Previous research has shown that decreased renal gluconeogenesis following kidney injury, which is also consistent with increased glycolysis and decreased mitochondrial pyruvate utilization, is associated with a worse prognosis [8,60]. However, our results suggest that this correlation is not causative and that an enhanced switch to glycolysis may be protective from severe rhabdomyolysis injury.

Our results also highlight mitochondrial pyruvate oxidation as contributing to AKI. AKI-dependent deactivating s-nitrosylation of pyruvate kinase M2 (PKM2) was previously found to increase PPP metabolites and protect from ischemia-reperfusion injury [12]. In contrast to inhibition of PKM2, decreasing MPC activity also impairs mitochondrial oxidation of circulating lactate. Circulating lactate is a major kidney fuel source [61] that bypasses kidney PKM2 and is converted to pyruvate by lactate dehydrogenase before mitochondrial import and oxidation. Our metabolomic data show that MPC disruption not only impairs pyruvate oxidation but increases kidney lactate levels, which was previously observed after AKI [9]. Beyond their role as fuels, pyruvate and lactate are chemical antioxidants, and when increased following AKI and in MPC TubKO mice could contribute to the AKI-protective effects we observed in MPC TubKO mice [62—66]. In accord, pyruvate administration during AKI has previously been shown to protect against kidney damage [10].

Our results reveal that tubular oxidative state is closely tied to MPC-dependent metabolism. The mitochondrial ETC maintains cellular ATP levels and produces physiologic ROS that informs metabolic regulation. However, perturbations in mitochondrial function can dysregulate ETC function and make it the primary cellular producer of pathological ROS [51,67]. Our observations that uninjured MPC TubKO mice have decreased Complex III activity, increased 3NT-modified proteins, and, in isolated MPC TubKO tubular cells, increased mitochondrial ROS production indicates that tubular MPC loss alters TCA cycle-ETC coupling. This could portend that tubular MPC disruption would be damaging to the kidney, especially during the extreme ROS burden of AKI. Indeed, glutathione depletion has been associated with increased oxidative damage in AKI [68], and delivery of AAV-glutathione reductase has been shown to protect from kidney damage [69]. However, the AKI-protective effects from MPC TubKO suggest that the increased antioxidant capacity induced by MPC disruption supersedes the primary metabolic stress imposed by it.

We note key limitations of this study and potential future areas of research interest. We do not address the rapid onset mechanism that downregulates *Mpc1* following AKI or the processes increasing glutathione reductase and thioredoxin reductase activities. Understanding these processes could influence novel preemptive approaches to protectively modulate tubular metabolism during AKI. Here, we utilized bolus injections of uniformly labeled ([U—^{13}C])-glucose or [U—^{13}C]-lactate/pyruvate to trace kidney metabolism in in vivo. While this non-steady state tracer approach can be highly effective and efficient for evaluating metabolism, it is more difficult to model, including accounting for secondary tracer effects. Future studies could use positionally-labeled tracers, employ infusions to reach a steady state, and be coupled with direct kidney perfusion or slice systems to parse the effects of MPC disruption with greater resolution. Next, given the continual discovery and development of MPC inhibitors like MSDC-0602 [70], zaprinast [71], new UK5099-like analogues [72], and non-indole inhibitors [73], modulating MPC activity pharmacologically as a preconditioning strategy or quickly after injury could be a potential approach to minimize AKI-dependent kidney damage. Finally, Pax8-dependent *Mpc1* knockout was not complete across all tubular segments. Thus, the stress of completely ablating MPC activity could be greater than we observed. Alternatively, the efficacy of MPC disruption to protect from AKI could be understated.

6. CONCLUSIONS

In conclusion, we show that kidney mitochondrial pyruvate uptake can be modulated to upregulate oxidant defense systems and protect from rhabdomyolysis-induced AKI. Our data support a model where MPC disruption elicits a goldilocks level of metabolic stress consistent with the concept of hormesis, where a mild, non-injurious stress upregulates stress defense systems, leading to protection from more severe stresses. Furthermore, MPC disruption induces an enhanced glycolytic shift following rhabdomyolysis that may decrease injury severity. Given the complexity of the mitochondrial transporter system and its relative lack of direct investigation in the kidney, we expect future research will reveal roles for mitochondrial fuel transport in both exacerbating and protecting from kidney injury and disease.

CREDIT AUTHORSHIP CONTRIBUTION STATEMENT

Adam J. Rauckhorst: Data curation, Formal analysis, Funding acquisition, Investigation, Methodology, Visualization, Writing — original draft, Writing — review & editing. **Gabriela Vasquez Martinez:** Data curation, Formal analysis, Investigation, Methodology, Visualization, Writing — original draft, Writing — review & editing. **Gabriel Mayoral Andrade:** Investigation, Writing — review & editing, Data curation. **Hsiang Wen:** Investigation, Writing — review & editing, Data curation. **Ji Young Kim:** Data curation, Investigation. **Aaron Simoni:** Data curation, Investigation, Writing — review & editing. **Claudia Robles-Planells:** Data curation, Investigation, Writing — review & editing. **Kranti A. Mapuskar:** Data curation, Investigation, Writing — review & editing. **Prerna Rastogi:** Data curation, Investigation, Writing — review & editing. **Emily J. Steinbach:** Data curation, Investigation, Writing — review & editing. **Michael L. McCormick:** Data curation, Investigation, Writing — review & editing, Funding acquisition. **Bryan G. Allen:** Formal analysis, Writing — review & editing, Funding acquisition. **Navjot S. Pabla:** Formal analysis, Methodology, Writing — review & editing. **Ashley R. Jackson:** Formal analysis, Investigation, Writing — review & editing. **Mitchell C. Coleman:** Methodology, Writing — review & editing, Funding acquisition. **Douglas R. Spitz:** Formal analysis, Methodology, Writing — original draft, Writing — review & editing, Funding acquisition. **Eric B. Taylor:** Conceptualization, Formal analysis, Funding acquisition, Methodology, Project administration, Supervision, Writing — original draft, Writing — review & editing, Data curation. **Diana Zepeda-Orozco:** Conceptualization, Data curation, Formal analysis, Funding acquisition, Methodology, Project administration, Resources, Supervision, Writing — original draft, Writing — review & editing.

DATA AVAILABILITY

Data will be made available on request.

ACKNOWLEDGEMENTS

This work was supported by grants CHD K12 HD027748 (DZO), NIH R01 DK104998 and the University of Iowa Healthcare Distinguished Scholars Award (EBT), ADA 1-18-PDF-060 and AHA CDA851976 (AJR), NIH P01 CA217797 and P30 CA086862 (DRS, BGA, KAM, MLM), NIDDK K01 DK126991 (ARJ), T32 DK007690 (EJS), and NIAMS R00 AR070914 (MCC).

DECLARATION OF COMPETING INTEREST

The authors declare no competing interests.

APPENDIX A. SUPPLEMENTARY DATA

Supplementary data to this article can be found online at https://doi.org/10.1016/j.molmet.2023.101849.

REFERENCES

[1] Chawla LS, Bellomo R, Bihorac A, Goldstein SL, Siew ED, Bagshaw SM, et al. Acute kidney disease and renal recovery: consensus report of the Acute Disease Quality Initiative (ADQI) 16 Workgroup. Nat Rev Nephrol 2017;13(4):241—57.

[2] Chertow GM, Burdick E, Honour M, Bonventre JV, Bates DW. Acute kidney injury, mortality, length of stay, and costs in hospitalized patients. J Am Soc Nephrol 2005;16(11):3365—70.

[3] Coca SG, Singanamala S, Parikh CR. Chronic kidney disease after acute kidney injury: a systematic review and meta-analysis. Kidney Int 2012;81(5):442—8.

[4] Goldstein SL, Jaber BL, Faubel S, Chawla LS. AKI transition of care: a potential opportunity to detect and prevent CKD. Clin J Am Soc Nephrol 2013;8(3):476—83.

[5] Bhargava P, Schnellmann RG. Mitochondrial energetics in the kidney. Nat Rev Nephrol 2017;13(10):629—46.

[6] Kaddourah A, Basu RK, Bagshaw SM, Goldstein SL, Investigators A. Epidemiology of acute kidney injury in critically ill children and young adults. N Engl J Med 2017;376(1):11—20.

[7] Grgic I, Campanholle G, Bijol V, Wang C, Sabbisetti VS, Ichimura T, et al. Targeted proximal tubule injury triggers interstitial fibrosis and glomerulosclerosis. Kidney Int 2012;82(2):172—83.

[8] Legouis D, Ricksten SE, Faivre A, Verissimo T, Gariani K, Verney C, et al. Altered proximal tubular cell glucose metabolism during acute kidney injury is associated with mortality. Nat Metab 2020;2(8):732—43.

[9] Lan R, Geng H, Singha PK, Saikumar P, Bottinger EP, Weinberg JM, et al. Mitochondrial pathology and glycolytic shift during proximal tubule atrophy after ischemic AKI. J Am Soc Nephrol 2016;27(11):3356—67.

[10] Zager RA, Johnson AC, Becker K. Renal cortical pyruvate depletion during AKI. J Am Soc Nephrol 2014;25(5):998—1012.

[11] Shen Y, Jiang L, Wen P, Ye Y, Zhang Y, Ding H, et al. Tubule-derived lactate is required for fibroblast activation in acute kidney injury. Am J Physiol Ren Physiol 2020;318(3):F689—701.

[12] Zhou HL, Zhang R, Anand P, Stomberski CT, Qian Z, Hausladen A, et al. Metabolic reprogramming by the S-nitroso-CoA reductase system protects against kidney injury. Nature 2019;565(7737):96—100.

[13] Scholz H, Boivin FJ, Schmidt-Ott KM, Bachmann S, Eckardt KU, Scholl UI, et al. Kidney physiology and susceptibility to acute kidney injury: implications for renoprotection. Nat Rev Nephrol 2021;17(5):335—49.

[14] Jang C, Chen L, Rabinowitz JD. Metabolomics and isotope tracing. Cell 2018;173(4):822—37.

[15] Bricker DK, Taylor EB, Schell JC, Orsak T, Boutron A, Chen YC. A mitochondrial pyruvate carrier required for pyruvate uptake in yeast, Drosophila, and humans. Science 2012;337(6090):96—100.

[16] Herzig S, Raemy E, Montessuit S, Veuthey JL, Zamboni N, Westermann B, et al. Identification and functional expression of the mitochondrial pyruvate carrier. Science 2012;337(6090):93—6.

[17] Vacanti NM, Divakaruni AS, Green CR, Parker SJ, Henry RR, Ciaraldi TP, et al. Regulation of substrate utilization by the mitochondrial pyruvate carrier. Mol Cell 2014;56(3):425—35.

[18] Yang C, Ko B, Hensley CT, Jiang L, Wasti AT, Kim J, et al. Glutamine oxidation maintains the TCA cycle and cell survival during impaired mitochondrial pyruvate transport. Mol Cell 2014;56(3):414—24.

[19] Schell JC, Wisidagama DR, Bensard C, Zhao H, Wei P, Tanner J. Control of intestinal stem cell function and proliferation by mitochondrial pyruvate metabolism. Nat Cell Biol 2017;19(9):1027—36.

[20] Grenell A, Wang Y, Yam M, Swarup A, Dilan TL, Hauer A, et al. Loss of MPC1 reprograms retinal metabolism to impair visual function. Proc Natl Acad Sci U S A 2019;116(9):3530—5.

[21] Fernandez-Caggiano M, Kamynina A, Francois AA, Prysyazhna O, Eykyn TR, Krasemann S, et al. Mitochondrial pyruvate carrier abundance mediates pathological cardiac hypertrophy. Nat Metab 2020;2(11):1223—31.

[22] McCommis KS, Kovacs A, Weinheimer CJ, Shew TM, Koves TR, Ilkayeva OR, et al. Nutritional modulation of heart failure in mitochondrial pyruvate carrier-deficient mice. Nat Metab 2020;2(11):1232—47.

[23] Zhang Y, Taufalele PV, Cochran JD, Robillard-Frayne I, Marx JM, Soto J, et al. Mitochondrial pyruvate carriers are required for myocardial stress adaptation. Nat Metab 2020;2(11):1248—64.

[24] Cluntun AA, Badolia R, Lettlova S, Parnell KM, Shankar TS, Diakos NA, et al. The pyruvate-lactate axis modulates cardiac hypertrophy and heart failure. Cell Metabol 2021;33(3):629–648 e10.
[25] Schell JC, Olson KA, Jiang L, Hawkins AJ, Van Vranken JG, Xie J, et al. A role for the mitochondrial pyruvate carrier as a repressor of the Warburg effect and colon cancer cell growth. Mol Cell 2014;56(3):400–13.
[26] Compan V, Pierredon S, Vanderperre B, Krznar P, Marchiq I, Zamboni N, et al. Monitoring mitochondrial pyruvate carrier activity in real time using a BRET-based biosensor: investigation of the Warburg effect. Mol Cell 2015;59(3):491–501.
[27] Gray LR, Sultana MR, Rauckhorst AJ, Oonthonpan L, Tompkins SC, Sharma A, et al. Hepatic mitochondrial pyruvate carrier 1 is required for efficient regulation of gluconeogenesis and whole-body glucose homeostasis. Cell Metabol 2015;22(4):669–81.
[28] McCommis KS, Chen Z, Fu X, McDonald WG, Colca JR, Kletzien RF, et al. Loss of mitochondrial pyruvate carrier 2 in the liver leads to defects in gluconeogenesis and compensation via pyruvate-alanine cycling. Cell Metabol 2015;22(4):682–94.
[29] Rauckhorst AJ, Gray LR, Sheldon RD, Fu X, Pewa AD, Feddersen CR, et al. The mitochondrial pyruvate carrier mediates high fat diet-induced increases in hepatic TCA cycle capacity. Mol Metabol 2017;6(11):1468–79.
[30] Sharma A, Oonthonpan L, Sheldon RD, Rauckhorst AJ, Zhu Z, Tompkins SC, et al. Impaired skeletal muscle mitochondrial pyruvate uptake rewires glucose metabolism to drive whole-body leanness. Elife 2019;8.
[31] Tompkins SC, Sheldon RD, Rauckhorst AJ, Noterman MF, Solst SR, Buchanan JL, et al. Disrupting mitochondrial pyruvate uptake directs glutamine into the TCA cycle away from glutathione synthesis and impairs hepatocellular tumorigenesis. Cell Rep 2019;28(10):2608–2619 e6.
[32] Bouchard M, Souabni A, Mandler M, Neubuser A, Busslinger M. Nephric lineage specification by Pax2 and Pax8. Genes Dev 2002;16(22):2958–70.
[33] Grouls S, Iglesias DM, Wentzensen N, Moeller MJ, Bouchard M, Kemler R, et al. Lineage specification of parietal epithelial cells requires beta-catenin/Wnt signaling. J Am Soc Nephrol 2012;23(1):63–72.
[34] Bai Y, Kim JY, Bisunke B, Jayne LA, Silvaroli JA, Balzer MS, et al. Kidney toxicity of the BRAF-kinase inhibitor vemurafenib is driven by off-target ferrochelatase inhibition. Kidney Int 2021;100(6):1214–26.
[35] Kim JY, Bai Y, Jayne LA, Cianciolo RE, Bajwa A, Pabla NS. Involvement of the CDKL5-SOX9 signaling axis in rhabdomyolysis-associated acute kidney injury. Am J Physiol Ren Physiol 2020;319(5):F920–9.
[36] Kim JY, Bai Y, Jayne LA, Hector RD, Persaud AK, Ong SS, et al. A kinome-wide screen identifies a CDKL5-SOX9 regulatory axis in epithelial cell death and kidney injury. Nat Commun 2020;11(1):1924.
[37] Kim JY, Jayne LA, Bai Y, Feng M, Clark MA, Chung S, et al. Ribociclib mitigates cisplatin-associated kidney injury through retinoblastoma-1 dependent mechanisms. Biochem Pharmacol 2020;177:113939.
[38] Pabla N, Gibson AA, Buege M, Ong SS, Li L, Hu S, et al. Mitigation of acute kidney injury by cell-cycle inhibitors that suppress both CDK4/6 and OCT2 functions. Proc Natl Acad Sci U S A 2015;112(16):5231–6.
[39] Rauckhorst AJ, Borcherding N, Pape DJ, Kraus AS, Scerbo DA, Taylor EB. Mouse tissue harvest-induced hypoxia rapidly alters the in vivo metabolome, between-genotype metabolite level differences, and (13)C-tracing enrichments. Mol Metabol 2022;66:101596.
[40] Fernandez CA, Des Rosiers C, Previs SF, David F, Brunengraber H. Correction of 13C mass isotopomer distributions for natural stable isotope abundance. J Mass Spectrom 1996;31(3):255–62.
[41] Spitz DR, Oberley LW. An assay for superoxide dismutase activity in mammalian tissue homogenates. Anal Biochem 1989;179(1):8–18.
[42] Ray LE, Prescott JM. Isolation and some characteristics of glutathione reductase from rabbit erythrocytes (38548). Proc Soc Exp Biol Med 1975;148(2):402–9.
[43] Glock GE, Mc LP. Further studies on the properties and assay of glucose 6-phosphate dehydrogenase and 6-phosphogluconate dehydrogenase of rat liver. Biochem J 1953;55(3):400–8.
[44] Barrientos A. In vivo and in organello assessment of OXPHOS activities. Methods 2002;26(4):307–16.
[45] Birch-Machin MA, Briggs HL, Saborido AA, Bindoff LA, Turnbull DM. An evaluation of the measurement of the activities of complexes I-IV in the respiratory chain of human skeletal muscle mitochondria. Biochem Med Metab Biol 1994;51(1):35–42.
[46] Kirita Y, Wu H, Uchimura K, Wilson PC, Humphreys BD. Cell profiling of mouse acute kidney injury reveals conserved cellular responses to injury. Proc Natl Acad Sci U S A 2020;117(27):15874–83.
[47] Kim JY, Bai Y, Jayne LA, Abdulkader F, Gandhi M, Perreau T, et al. SOX9 promotes stress-responsive transcription of VGF nerve growth factor inducible gene in renal tubular epithelial cells. J Biol Chem 2020;295(48):16328–41.
[48] Nizar JM, Shepard BD, Vo VT, Bhalla V. Renal tubule insulin receptor modestly promotes elevated blood pressure and markedly stimulates glucose reabsorption. JCI Insight 2018;3(16).
[49] Halestrap AP. The mitochondrial pyruvate carrier. Kinetics and specificity for substrates and inhibitors. Biochem J 1975;148(1):85–96.
[50] Nieth H, Schollmeyer P. Substrate-utilization of the human kidney. Nature 1966;209(5029):1244–5.
[51] Chouchani ET, Pell VR, Gaude E, Aksentijevic D, Sundier SY, Robb EL, et al. Ischaemic accumulation of succinate controls reperfusion injury through mitochondrial ROS. Nature 2014;515(7527):431–5.
[52] Goodman RP, Markhard AL, Shah H, Sharma R, Skinner OS, Clish CB, et al. Hepatic NADH reductive stress underlies common variation in metabolic traits. Nature 2020;583(7814):122–6.
[53] Thompson Legault J, Strittmatter L, Tardif J, Sharma R, Tremblay-Vaillancourt V, Aubut C, et al. A metabolic signature of mitochondrial dysfunction revealed through a monogenic form of leigh syndrome. Cell Rep 2015;13(5):981–9.
[54] Bowman CE, Zhao L, Hartung T, Wolfgang MJ. Requirement for the mitochondrial pyruvate carrier in mammalian development revealed by a hypomorphic allelic series. Mol Cell Biol 2016;36(15):2089–104.
[55] Lu SC. Glutathione synthesis. Biochim Biophys Acta 2013;1830(5):3143–53.
[56] Petejova N, Martinek A. Acute kidney injury due to rhabdomyolysis and renal replacement therapy: a critical review. Crit Care 2014;18(3):224.
[57] Giustarini D, Dalle-Donne I, Milzani A, Braconi D, Santucci A, Rossi R. Membrane skeletal protein S-glutathionylation in human red blood cells as index of oxidative stress. Chem Res Toxicol 2019;32(6):1096–102.
[58] Schafer FQ, Buettner GR. Redox environment of the cell as viewed through the redox state of the glutathione disulfide/glutathione couple. Free Radic Biol Med 2001;30(11):1191–212.
[59] Gewin LS. Sugar or fat? Renal tubular metabolism reviewed in health and disease. Nutrients 2021;13(5).
[60] Verissimo T, Faivre A, Rinaldi A, Lindenmeyer M, Delitsikou V, Veyrat-Durebex C, et al. Decreased renal gluconeogenesis is a hallmark of chronic kidney disease. J Am Soc Nephrol 2022;33(4):810–27.
[61] Hui S, Ghergurovich JM, Morscher RJ, Jang C, Teng X, Lu W, et al. Glucose feeds the TCA cycle via circulating lactate. Nature 2017;551(7678):115–8.
[62] Groussard C, Morel I, Chevanne M, Monnier M, Cillard J, Delamarche A. Free radical scavenging and antioxidant effects of lactate ion: an in vitro study. J Appl Physiol 2000;89(1):169–75.
[63] Guarino VA, Oldham WM, Loscalzo J, Zhang YY. Reaction rate of pyruvate and hydrogen peroxide: assessing antioxidant capacity of pyruvate under biological conditions. Sci Rep 2019;9(1):19568.
[64] Tauffenberger A, Fiumelli H, Almustafa S, Magistretti PJ. Lactate and pyruvate promote oxidative stress resistance through hormetic ROS signaling. Cell Death Dis 2019;10(9):653.

[65] Ramos-Ibeas P, Barandalla M, Colleoni S, Lazzari G. Pyruvate antioxidant roles in human fibroblasts and embryonic stem cells. Mol Cell Biochem 2017;429(1–2):137–50.
[66] Wang X, Perez E, Liu R, Yan LJ, Mallet RT, Yang SH. Pyruvate protects mitochondria from oxidative stress in human neuroblastoma SK-N-SH cells. Brain Res 2007;1132(1):1–9.
[67] Liu Y, Fiskum G, Schubert D. Generation of reactive oxygen species by the mitochondrial electron transport chain. J Neurochem 2002;80(5):780–7.
[68] Shang Y, Siow YL, Isaak CK, Karmin O. Downregulation of glutathione biosynthesis contributes to oxidative stress and liver dysfunction in acute kidney injury. Oxid Med Cell Longev 2016;2016:9707292.
[69] Gao D, Wang S, Lin Y, Sun Z. In vivo AAV delivery of glutathione reductase gene attenuates anti-aging gene klotho deficiency-induced kidney damage. Redox Biol 2020;37:101692.
[70] Vigueira PA, McCommis KS, Hodges WT, Schweitzer GG, Cole SL, Oonthonpan L, et al. The beneficial metabolic effects of insulin sensitizers are not attenuated by mitochondrial pyruvate carrier 2 hypomorphism. Exp Physiol 2017;102(8):985–99.
[71] Du J, Cleghorn WM, Contreras L, Lindsay K, Rountree AM, Chertov AO, et al. Inhibition of mitochondrial pyruvate transport by zaprinast causes massive accumulation of aspartate at the expense of glutamate in the retina. J Biol Chem 2013;288(50):36129–40.
[72] Hegazy L, Gill LE, Pyles KD, Kaiho C, Kchouk S, Finck BN, et al. Identification of novel mitochondrial pyruvate carrier inhibitors by homology modeling and pharmacophore-based virtual screening. Biomedicines 2022;10(2).
[73] Liu X, Flores AA, Situ L, Gu W, Ding H, Christofk HR, et al. Development of novel mitochondrial pyruvate carrier inhibitors to treat hair loss. J Med Chem 2021;64(4):2046–63.

